Novel Modeling and Nonlinear Control of the Siwakoti-H Inverter Considering Flying Capacitor Voltage Balance for Photovoltaic Applications

A. M. Mohammadi¹ N. R. Abjadi² G. R. Arab Markadeh³

Faculty of Engineering, Shahrekord University, Shahrekord, Iran. ^{1,2}
Department of Electrical Engineering, Faculty of Engineering, Ferdowsi University of Mashhad, Mashhad, Iran. ³
Corresponding author's email: abjadi.navidreza@sku.ac.ir

Article Info

ABSTRACT

Article type:

Research Article

Article history:

Received: 31-January-2025 Received in revised form: 16-March-2025

Accepted: 03-April-2025 Published online: 23-Sep-2025

Keywords:

feedback linearization, flying capacitor, photovoltaic, Siwakoti-H inverter.

The Siwakoti-H inverter (SHI) with a flying capacitor is a recent addition to the transformerless inverter family, suitable for grid-connected single-phase photovoltaic systems. It offers a promising alternative to traditional topologies without the need for transformers, due to its minimal power electronic components. However, one of the key challenges in managing flying capacitor (FC) inverters is ensuring that the voltage of the FC remains within the desired range. Materials and Methods: To tackle this issue, first, a novel nonlinear model of the SHI is obtained defining two control inputs and two control outputs, and then a nonlinear feedback linearization (FBL) control design is proposed for the SHI when connected to a single-phase grid. This article introduces a novel approach to the modeling and control of the SHI enabling simultaneous control of both the injected current to the grid and the flying capacitor voltage. The proposed modeling and the designed control method play a crucial role in maintaining the capacitor voltage within the specified range and in tracking a sinusoidal reference for the injected current into the single-phase network. A PWM implementation of the proposed control is also suggested which is useful in the practical setup. The obtained model can be extended for the SHI with other line filters and it can be used to design more sophisticated controllers for SHI. The simulation and practical results presented in this study demonstrate the effectiveness of the proposed modeling and control approach.

I. Introduction

Power electronics converters play a crucial role in converting and regulating electric power in grid-connected renewable energy systems through the switching patterns [1]. The focus on renewable energy systems, such as wind turbines and photovoltaic systems has been on achieving high efficiency over the past decade [2-4]. In [3], a microgrid with renewable energy sources is investigated and complicated controllers are designed. In [4], a power system with some distributed wind resources is considered and some sophisticated nonlinear controllers are designed for the system.

To minimize losses within the system, utilizing converter topologies with fewer switching elements is essential. In

addition, there is a growing tendency in photovoltaic systems towards not using transformers in converters [5-6]. Transformerless inverter has higher efficiency, less weight and lower cost compared to inverter with transformer; however, conventional single-phase grid-connected photovoltaic systems suffer from leakage current [7]. Besides safety issue, the leakage current increases grid ripples, photovoltaic system electromagnetic interference (EMI) [8]. The leakage current is more investigated in [9]. In [10-12], three multi-level switched-capacitor inverters are proposed which are not suitable for grid-connected transformerless photovoltaic application due to the issue of leakage current. In [13], a fifteen-level inverter which has several DC sources and suffers from leakage current.

There are various transformerless single-phase inverters which eliminate or reduce leakage current such as HERIC, H5, H6 [14, 8]; however, compared to conventional H-bridge inverter, these inverters have additional switches; some of them need special modulations or can't inject reactive power to the grid. In [15], an H-bridge less grid-tied multilevel inverter is proposed which reduce the leakage current significantly; however, it cannot be built with the available conventional H-bridges.

Some of the configurations use common ground to omit the leakage current. In these configurations the negative end of the solar panel is connected to the grid neutral directly. In [16] and [17] two common ground transformerless inverters are proposed which have simple configurations. They have an additional capacitor compared to conventional H bridge inverter. This capacitor is called the flying capacitor (FC). The inverter in [17] is called Siwakoti H inverter (SHI). There are three types of single-phase inverters with FC for photovoltaic grid-connected applications: Type-I, which has two switches in series during positive cycle [18]. This type can be implemented using two half-bridges and an additional diode. Type-II, which has a single switch in series during the positive cycle [18]. The components of this type are the same as those of type-I. Type-III or SHI which is discussed in this paper. Other types of single-phase inverters for photovoltaic grid-connected applications are reviewed in [19].

The SHI is a notable transformerless inverter topology that has gained attention [18]. This innovative design, which consists of only four switches, operates based on the flying capacitor principle [17]. What sets this topology apart is its ability to meet the needs of both positive and negative voltage sources using a single flying capacitor. Consequently, the number of the input voltage sources is reduced in comparison to the three-level neutral point clamp converter. Compared to the conventional H-bridge inverter, the SHI eliminates leakage current while using the same number of switches and a very similar topology. Compared to the HERIC, the SHI has less components and it can also inject reactive power to the grid without any special modulation technique. For a single-phase photovoltaic system, it is noteworthy that the nominal power is limited to 5KVA and given the relatively high costs of the solar power system, it is usually preferred to inject only active power into the grid. In the past, the operation of the grid-connected SHI was analyzed using a state feedback controller [20]. While the controller demonstrated satisfactory steady-state performance for the mentioned converter, it exhibited a noticeable deviation near the zero crossing of injected current to the grid. Besides, the FC voltage is decreased during the discharge state. This phenomenon can be attributed to the abrupt transition of the power from the input source to the floating capacitor. To address this issue and enhance the dynamic response, an alternative approach,

utilizing direct/indirect model predictive control (MPC) strategy for a grid-connected SHI has been suggested in [21-22]. Both papers address the unbalancing issue of the FC voltage; however, the presented controls are not perfect. Considering a cost function to control the injected current and the FC voltage simultaneously is not enough to achieve perfect tracking and selection of the weights in the cost function is also difficult. In addition, despite the offline computation, the computation in the controllers is still high, which consumes DSP time.

Nonlinear control methods address complex challenges by analyzing and designing systems with nonlinear components [23-24]. They offer diverse and powerful techniques, established in industrial applications. Feedback linearization methods, such as input-output feedback linearization (IOFL), solve the tracking problem in many systems and provide the stability of the closed-loop system [25]. In this paper, first a suitable model is obtained for SHI, then using this model an IOFL control is designed to achieve injected current reference tracking and the FC voltage balancing.

The organization of the paper is as follows: In section II the SHI is described and its operation is discussed. A new modeling of SHI is obtained in section III. A nonlinear controller is designed for SHI in section IV. Simulation and practical results are shown in sections IV and V respectively. Finally the conclusions are provided in section VI.

II. SHI description and operation

The circuit diagram of the SHI connected to a single-phase grid is depicted in Fig. 1. The SHI consists of four power switches and a capacitor, as shown in Fig. 1. Among these switches, S1 and S4 function as bipolar voltage blocking switches, while S2 and S3 serve as unipolar voltage blocking switches [17]. Consequently, switches S2 and S3 are implemented using MOSFETs or IGBTs, whereas switches S1 and S4 are implemented using a reverse blocking IGBTs (RB-IGBTs) or MOSFETS with blocking diodes. C_F is the FC. Since the polarity of the voltage across the FC does not change and it must be large enough to store energy to generate the negative voltage, a polarized electrolytic capacitor can be used as the FC. There is no need for an AC capacitor to serve as the FC. The inductance L is used as a filter to connect the inverter to the grid. As it is seen, the negative end of the input source is connected to the neutral of the grid and the DC and AC sections have a common

TABLE I THE STATES OF THE SHI SWITCHES FOR THE OPERATIONAL MODES

Mode	S1	S2	S3	S4
P	0	0	1	0
Z	1	0	0	1
N	0	1	0	0

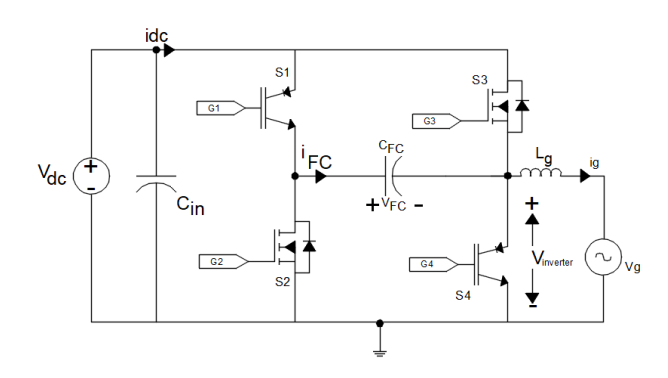


Fig. 1. The SHI connected to a single-phase grid

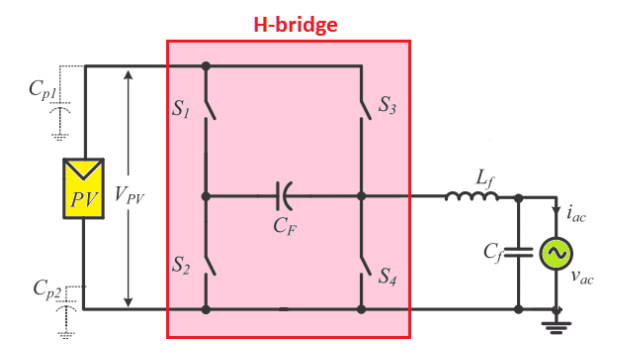


Fig. 2. The SHI fed from a photovoltaic panel and the parasitic capacitors

In Fig. 2, it is shown when the source is a photovoltaic panel, using the common ground, the parasitic capacitors of the panel cannot generate leakage current. In fact, the parasitic capacitor connected to the negative end is short circuited and the parasitic capacitor connected to the positive end has a constant voltage and its current equals zero.

A notable characteristic of this configuration is the utilization of the input DC source to fulfill the negative voltage required for the negative mode. This is accomplished by cyclically charging and discharging the FC, resulting in a virtual negative forward link, as illustrated in Figure 3.

The operation of the SHI can be described in three modes: positive (P) mode, negative (N) mode, and zero (Z) mode, as depicted in Fig. 4. During the P and N modes, switches S3 and S2 are activated, respectively. In the Z mode, switches S1 and S4 are activated to provide the zero voltage at the output and to charge the FC.

III. Modeling of the SHI

The three operational modes of the SHI are summarized in Table I. For each of these modes, an equivalent circuit can be obtained which are shown in Fig. 5. In the following,

considering the FC voltage ($^{\chi_1}$) and the inductor current (

 x_2) as state variables, the state-space equations of each mode is obtained; then these equations are combined to achieve the average model of the SHI.

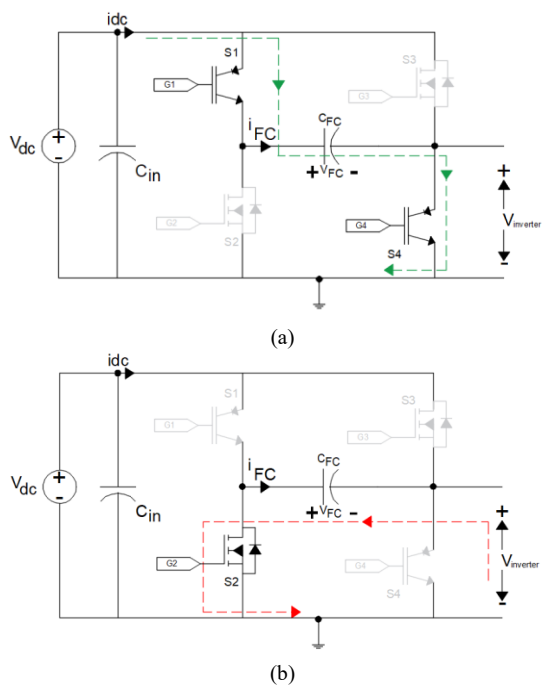


Fig. 3. Illustration of the charging and discharging of the FC, a) charging mode b) discharging mode wherein the capacitor uses as a virtual negative DC-link.

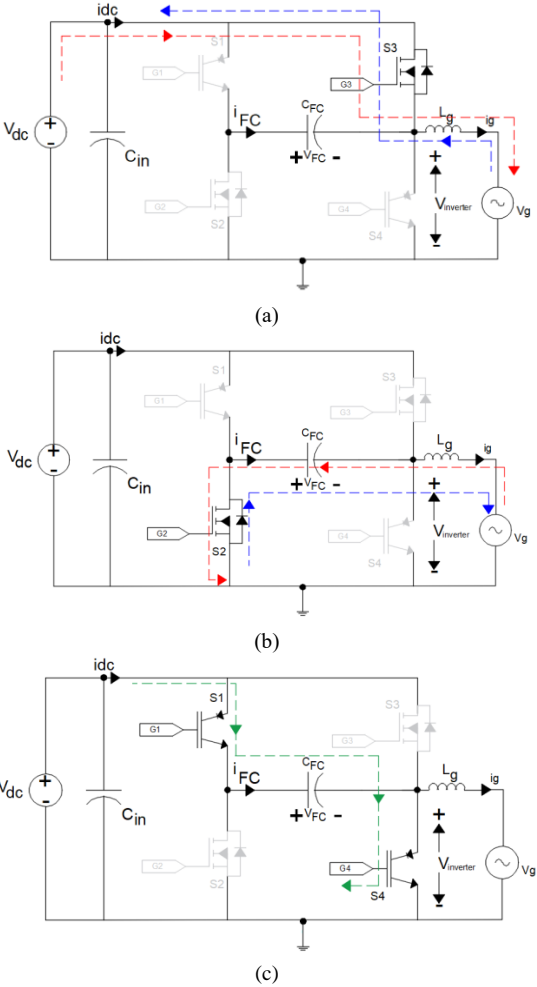
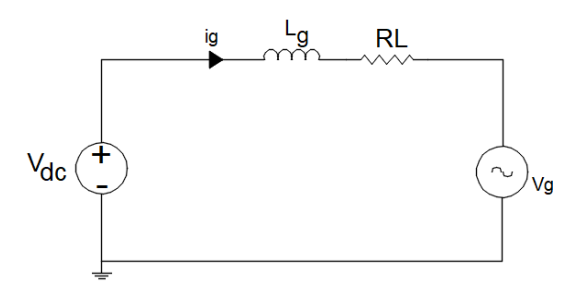
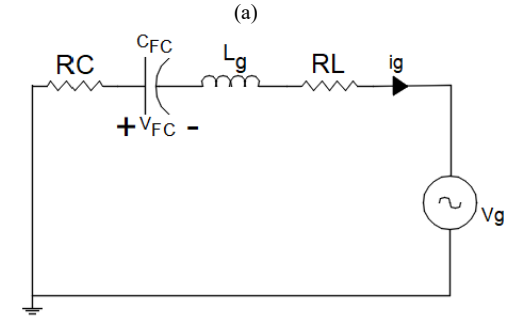
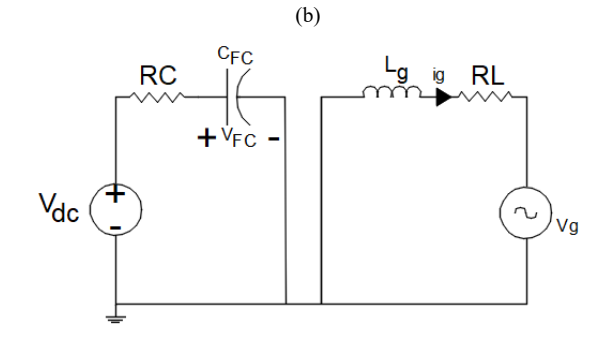


Fig. 4. The three operational modes of the SHI: a) P mode b) N mode c) Z mode







(c)
Fig. 5. The equivalent circuits of the SHI: a) P mode b) N mode c) Z mode

A. P mode

Referring to Fig. 5.a and using Kirchhoff voltage/current laws, one can obtain

$$i_{C_{FC}} = 0 \tag{1}$$

$$V_{dc} = Lg \frac{di_L}{dt} + R_L i_g + V_g \tag{2}$$

where R_L is the equivalent series resistance (ESR) of the inductor

These equations can be rewritten as

$$\dot{x}_1 = 0 \tag{3}$$

$$\dot{x}_{2} = \frac{V_{dc} - V_{g} - R_{L} x_{2}}{Lg} \tag{4}$$

B. N mode

Referring to Fig. 5.b and using Kirchhoff voltage/current laws, one can obtain

$$i_{C_{FC}} = i_g \tag{5}$$

$$V_{C_{FC}} + V_L + V_{Lg} + (R_C + R_L)i_g = 0$$
(6)

where R_C is the ESR of the FC.

These equations can be rewritten as

$$\dot{x}_1 = \frac{x_2}{C_{FC}} \tag{7}$$

$$\dot{x}_2 = \frac{-V_g - x_1 - (R_C + R_L)x_2}{Lg} \tag{8}$$

C. Z mode

Referring to Fig. 5.c and using Kirchhoff voltage/current laws, one can obtain

$$-V_{dc} + V_{C_{FC}} + R_{c} i_{C_{FC}} = 0 (9)$$

$$R_{L}i_{L} + V_{L} + V_{\sigma} = 0 (10)$$

These equations can be rewritten as

$$\dot{x}_1 = \frac{V_{dc} - x_1}{R_C C_{FC}} \tag{11}$$

$$\dot{x}_2 = \frac{-V_g - R_L x_2}{Lg} \tag{12}$$

D. Average model

To obtain the average model, the following duty-cycles are defined for P, N and Z modes:

$$u^+ = \frac{t^+}{T} \tag{13}$$

$$u^{-} = \frac{t^{-}}{T} \tag{14}$$

$$u^0 = \frac{t^0}{T} \tag{15}$$

where t^+ , t^- and t^0 are the time intervals of P, N and Z modes respectively; T is the switching period.

It is notable that

$$u^{+} + u^{-} + u^{0} = 1 \tag{16}$$

Multiply (3)-(4), (7)-(8) and (11)-(12) by (13), (14) and (15) respectively. From the sum of the results and using (16), it is concluded that:

$$\dot{x} = A + BW \tag{17}$$

where

$$A = \begin{bmatrix} \frac{V_{dc} - x_1}{R_C C_{FC}} \\ \frac{-V_g - R_L x_2}{Lg} \end{bmatrix}$$
 (18)

$$B = \begin{bmatrix} \frac{x_1 - V_{dc}}{C_{FC} R_C} & \frac{x_1 - V_{dc}}{C_{FC} R_C} + \frac{x_2}{C_{FC}} \\ \frac{V_{dc}}{Lg} & \frac{-x_1 - R_C x_2}{Lg} \end{bmatrix}$$
(19)

$$\boldsymbol{x}^T = \begin{bmatrix} \boldsymbol{V}_{C_{FC}} & \boldsymbol{i}_g \end{bmatrix} \tag{20}$$

$$W^{T} = \begin{bmatrix} u^{+} & u^{-} \end{bmatrix} \tag{21}$$

where W is the control input vector.

It is notable that (17) is a nonlinear system.

IV. FBL control

The SHI exhibits nonlinear behavior due to the product of the state and input variables. In this section, using the new model obtained in (17), a FBL controller is designed for SHI. The FBL controller is designed based on the input-output linearization. The basic approach of input-output linearization is simply to differentiate the outputs functions repeatedly until the inputs appear and then design the inputs to cancel the nonlinearity and the coupling.

A. FBL controller design

Define the following tracking errors:

$$e_1 = x_1 - x_1^*$$

$$e_2 = x_2 - x_2^*$$

where x_1^* and x_2^* are reference values. One can consider e_1 and e_2 as new outputs and their desired values are 0.

Differentiating (22) and (23) with respect to time and substituting from (17), one can obtain:

$$\dot{e}_1 = \dot{x}_1 - \dot{x}_1^* = a_1 + b_{11}u^+ + b_{12}u^-$$

$$- \dot{x}_1^*$$
(22)

$$\dot{e}_2 = \dot{x}_2 - \dot{x}_2^* = a_2 + b_{21}u^+ + b_{22}u^-$$

$$- \dot{x}_2^*$$
(23)

where a_i and b_{ij} are the elements of (18) and (19) respectively.

By equating (22) with $-k_1e_1$ and (23) with $-k_2e_2$, the result is:

$$\dot{e}_1 + k_1 e_1 = 0 \tag{24}$$

$$\dot{e}_2 + k_2 e_2 = 0 \tag{25}$$

By choosing positive coefficients k_1 and k_2 , the errors converge to zero exponentially.

By comparing (22) with (24) and (23) with (25), it is concluded that:

$$u = \begin{bmatrix} u^+ \\ u^- \end{bmatrix} = B^{-1} (\begin{bmatrix} \dot{x}_1^* \\ \dot{x}_2^* \end{bmatrix} - A - \begin{bmatrix} k_1 e_1 \\ k_2 e_2 \end{bmatrix}) \tag{26}$$

Eq. (26) is the FBL control law. Selecting k_i s large enough, the errors converge to zero rapidly.

B. Stability analysis

The system described by (17) or (22)-(23) is a multi-input multi-output (MIMO) square system with two inputs (u^- , u^+) and two outputs (e_1 , e_2). The system order n is 2. The number r_i of differentiations required for one of the inputs (u^- , u^+) to appear in the derivatives of output e_i is called the relative degree of the corresponding subsystem. For the MIMO system the relative degree is $(r_1, r_2) = (1,1)$. The total relative degree is $r = r_1 + r_2 = 2$ which is equal to the system order n=2. In this case, there is no internal dynamics. The control law (26) guarantees the exponential convergence of errors to 0 without any need to worry about the stability of the internal dynamics or zero dynamics. Based on the fact that there is no zero dynamic, the system is also a minimum phase system [23].

To check the singularity of the proposed controller, the determinant of matrix B in (19) is obtained:

$$\det(B) = \frac{1}{L_g C_{FC} R_C} (2V_{dc} x_1 + 2V_{dc} R_C x_2 - x_1^2 - R_C x_1 x_2 + V_{dc}^2)$$
(27)

This determinant rarely becomes zero.

Assuming $x_1 \approx V_{dc}$ one can obtain:

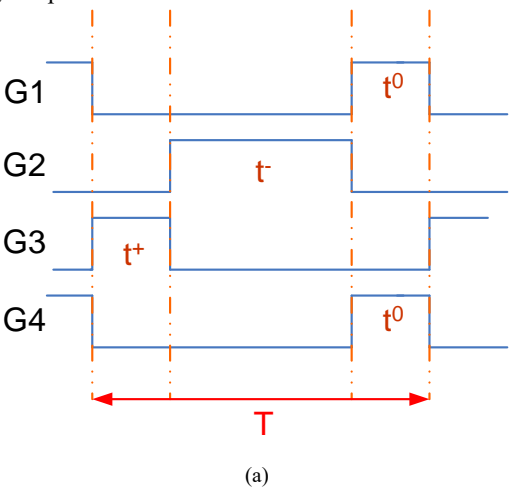
$$\det(B) \approx \frac{1}{L_a C_{FC} R_C} (2V_{dc}^2 + V_{dc} R_C x_2)$$
 (28)

Moreover, assuming $|R_C x_2| \ll V_{dc}$ it is concluded that:

$$\det(B) \approx \frac{1}{L_a C_{FC} R_C} (2V_{dc}^2) > 0$$
 (29)

C. Implementation Dwell times with PWMS

To implement this control law using PWM technique, one can consider the following procedure. The gates pulses based on t^+ , t^- and t^0 are shown in Fig. 6.a. Comparing the pulses in Fig. 6.a and the PWM signals in Fig. 6.b, one can obtain the gates pulses as:



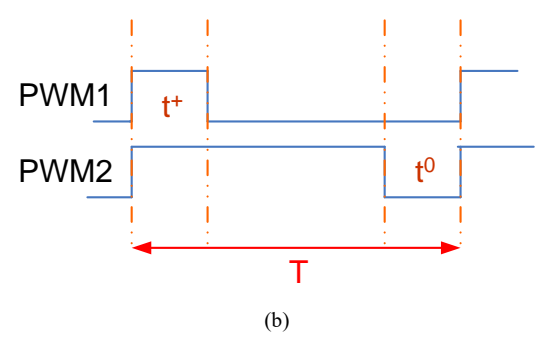


Fig. 6. Dwell times and PWM pulses, a) gates pulses, b) PWM signals

$$G_1 = G_4 = \overline{PWM}_2 \tag{30}$$

$$G_2 = \overline{PWM}_1 \bigwedge PWM_2 \tag{31}$$

$$G_3 = PWM_1 \tag{32}$$

V. Simulation results

To show the validity and the effectiveness of the proposed model and the proposed controller, some simulation results are obtained using PSIM software. Details of the parameters used in all simulation runs are provided in Table II.

In Fig. 7 the simulation results of PI control without controlling the FC voltage is presented. It is seen that the FC voltage changes a lot, which can cause problems for the inverter. Even the overall closed-loop system may become unstable.

In Fig. 8 the simulation results of FBL control are presented. It is seen that the injected current to the grid tracks its reference perfectly. The FC voltage is also near its reference; however it has pulsations. This phenomenon is due to the instantaneous power at the single-phase ac port, which pulsates at twice the AC voltage frequency, generating the second harmonic current at the DC bus.

FBL does not inherently account for the uncertainties, making it less robust in practical scenarios where exact

TABLE II SHI AND CONTROLLER PARAMETERS VALUES

Parameter	Value	
DC input voltage	20 v	
Switching frequency	2 KHz	
Line frequency	50 Hz	
FC	1000 μF-35v	
Filter inductor	20 mH	
$r_{\!\scriptscriptstyle L}$	1Ω	
r_{C}	1 Ω	
	250	
k_2	9500	
· · · · · · · · · · · · · · · · · · ·		

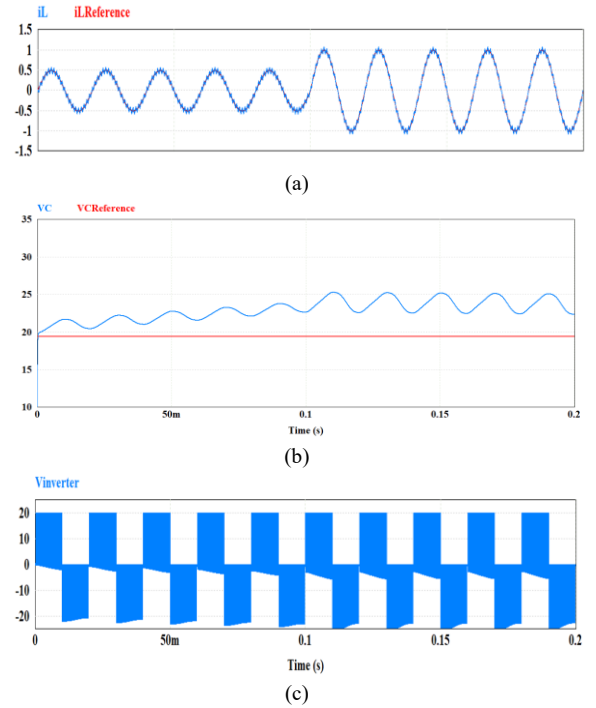
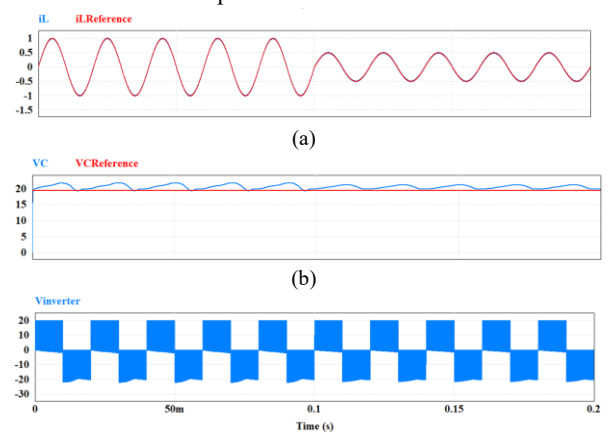


Fig. 7. The simulation results of PI control without FC voltage control, a) the injected current and its reference, b) the FC voltage and its reference, c) the inverter voltage

system parameters are unknown or subject to variation. To demonstrate the resilience of the designed control, an additional simulation test has been added, considering a 20% error in the values of the FC and the inductor. The results of this test are presented in Fig. 9. It is seen with small inaccuracy in the parameters, small deviations are appeared between the responses and their references. To achieve a robust control, the designed FBL control should be combined with sliding mode control or adaptive control techniques.

VI. Experimental results

Fig. 10 shows the experimental setup. To implement the proposed controller a Discovery board is used. It has a 32 bit STM32F407 microcontroller. This microcontroller has 1 MB of Flash memory, 192 KB of RAM, 17 timers, 3 ADCs and 2 DACs. This device provides a 168 MHz/210 DMIPS



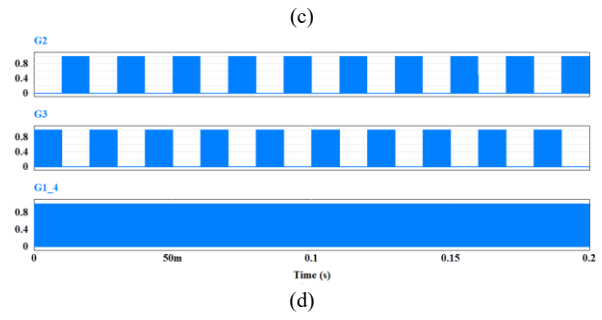


Fig. 8. The simulation results of FBL control, a) the injected current and its reference, b) the FC voltage and its reference, c) the inverter voltage, d) the pulses of gates

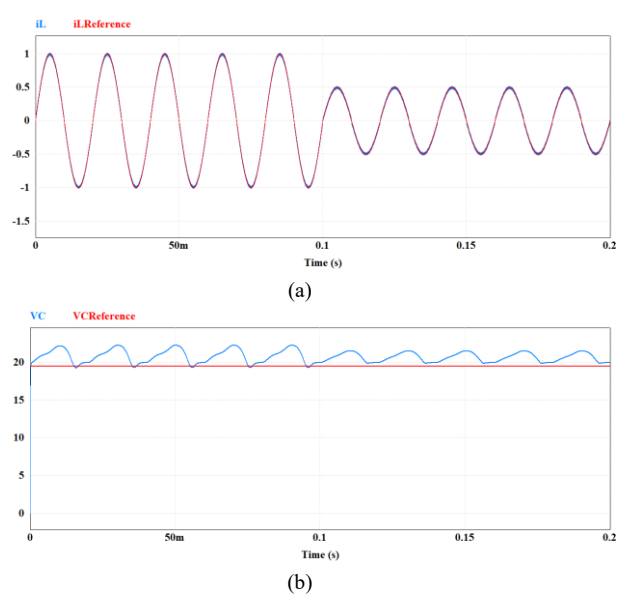


Fig. 9. The simulation results of FBL control with 20% error in some parameters, a) the injected current and its reference, b) the FC voltage and its reference

Cortex-M4 with single cycle DSP MAC and floating point unit suitable to measure the required variables and to implement the nonlinear controller.

Two signals are measured and fed back to the control

system: the FC voltage (X_1) and the inductor current (X_2). The advantage of feeding back of these two variables is the simultaneous control of the FC voltage and the injected current into the grid.

In Fig. 11 the obtained practical results using the proposed FBL control are shown. In Figs. 11.a and 11.b, the injected current and its reference are shown in both increase and decrease of the injected current. In both case, the injected current tracks its reference. In Fig. 11.c the FC voltage is shown during the increase of the injected current. The ripple on FC voltage is from second order harmonics in single-phase system and it is increased when the injected current is increased as seen in the Fig. 11.c. Using the proposed FBL control, the FC voltage does not deviate. The DC voltage input is also shown in Fig. 11.d



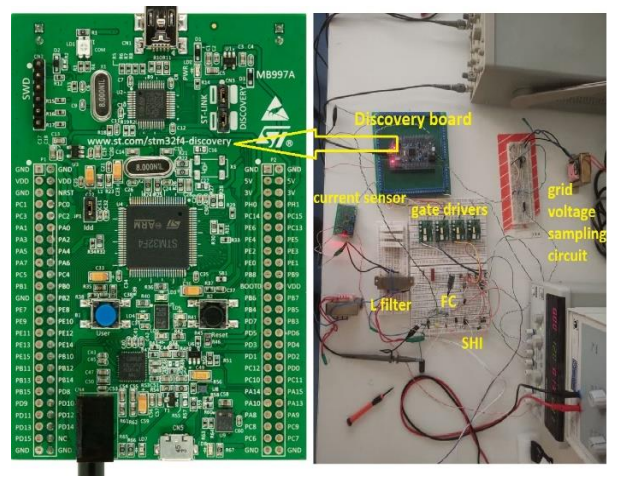
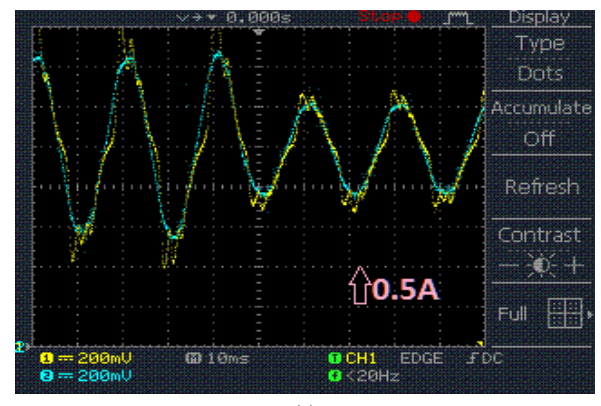
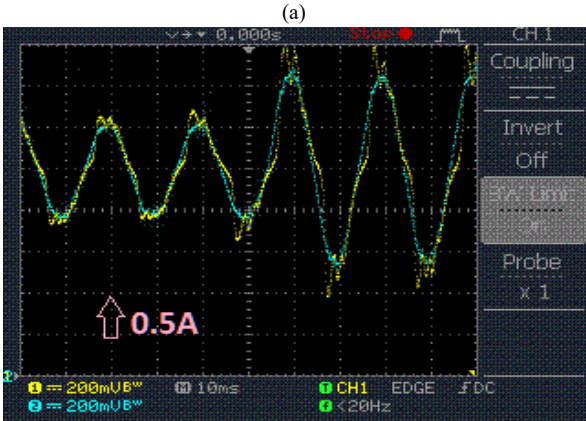


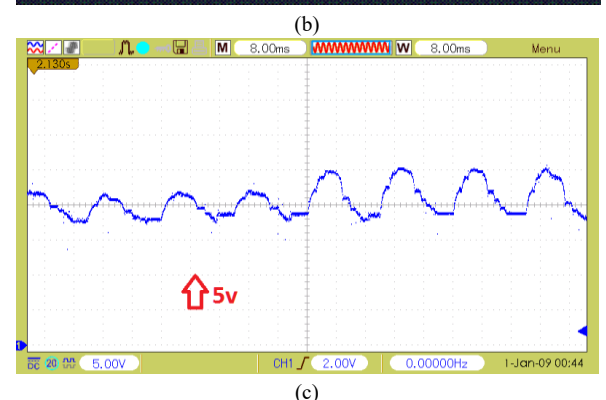
Fig. 10. The experimental setup

VII. Conclusions

In this paper, a new model is developed for the SHI. A novel controller for the SHI is proposed based on the FBL control. The deviation of the FC voltage is investigated and it is demonstrated that such deviations can be avoided using the proposed control. The proposed control is compared with conventional PI control and it is shown that the proposed controller can control the injected current and the FC voltage simultaneously. To implement the proposed control using PWM techniques, particularly in practical setups, an innovative method is suggested. Simulation and practical results are obtained and the superiority and effectiveness of the proposed modeling and control are verified. It is observed that although the experimental results are slightly less accurate than the simulation results, the overall patterns of the outcomes remain consistent. The innovative obtained model of the SHI can be used to design more sophisticated controllers. To improve robustness, the FBL control can be combined with robust control techniques such as adaptive control or sliding mode control techniques in future research works.







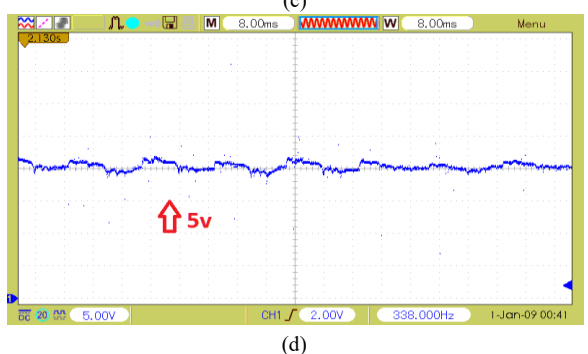


Fig. 11. The practical results, a) increasing current, b) decreasing current, c) FC voltage, d) input DC voltage

REFERENCES

 L. A. Kumar, S. A. Alexander, M. Rajendran, Power Electronic Converters for Solar Photovoltaic Systems, Academic Press, 2020, doi: 10.1016/C2019-0-04270-7.

- [2] I. Dincer, M. Temiz, Renewable Energy Options for Power Generation and Desalination, Springer, 2024, doi: 10.1007/978-3-031-53437-9.
- [3] N. R. Abjadi, "Adaptive Input-Output Feedback Linearization Control for Islanded Inverter-Based Microgrids," International Journal of Industrial Electronics, Control and Optimization (IECO), Vol. 6, No. 3, 2023, doi: 10.22111/ieco.2023.44787.1465.
- [4] S. Abazari, "Novel Non-linear Control of DFIG and SSSC for Stability Increment of Power System," International Journal of Industrial Electronics, Control and Optimization (IECO), Vol. 7, No. 1, 2024, 10.22111/ieco.2023.45795.1485.
- [5] H. Xiao, X. Wang, Transformerless Photovoltaic Grid-Connected Inverters, Springer, 2021, doi: 10.1007/978-981-15-8525-8.
- [6] M. Farhadi-Kangarlu, F. Mohammadi, "Performance Improvement of Single-Phase Transformer less Grid-Connected PV Inverters Regarding the CMV and LVRT," Journal of Operation and Automation in Power Engineering, Vol. 7, No. 1, 2019, doi: 10.22098/JOAPE.2019.4366.1344.
- [7] Md. F. Kibria, A. Elsanabary, K. S. Tey, M. Mubin, S. Mekhilef, "A Comparative Review on Single Phase Transformerless Inverter Topologies for Grid-Connected Photovoltaic Systems," Energies, Vol. 16, No. 1362, 2023, doi: 10.3390/en16031363.
- [8] T. K. S. Freddy, N. A. Rahim, W.-P. Hew, H. S. Che, "Comparison and Analysis of Single-Phase Transformerless Grid-Connected PV Inverters," IEEE Transactions on Power Electronics, Vol. 29, No. 10, 2014, doi: 10.1109/TPEL.2013.2294953.
- [9] H. Xiao, S. Xie, "Leakage Current Analytical Model and Application in Single-Phase Transformerless Photovoltaic Grid-Connected Inverter," IEEE Transaction on Electromagnetic Compability, Vol. 52, No. 4, 2010, doi: 10.1109/TEMC.2010.2064169.
- [10] M. Derakhshandeh, M. Hosseinpour, A. Seifi, M. Shahparasti, "An enhanced 13-level triple voltage gain switched capacitor inverter with lower power electronics devices," IET Power Electronics, 2024, doi: 10.1049/pel2.12748.
- [11] A. Vijayakumar, A. A. Stonier, G. Peter, E. Vignesh, V. Ganji, "Machine learning based model predictive control for grid connected enhanced switched capacitor cross-connected switched multi-level inverter (ESC3SMLI)," IET Power Electronics, 2023, doi: 10.1049/pel2.12546.
- [12] M. Noori, M. Hosseinpour, S. R. Mousavi-Aghdam, "Single Source Switched Capacitor Multilevel inverter with Voltage Boosting Capability and Low Switch Count," Journal of Iranian Association of Electrical and Electronics Engineers (JIAEEE), No. 2, 2024, doi: 10.61186/jiaeee.21.2.47.
- [13] Y. Joshi, S. S. Letha, F. I. Bakhsh, G. L. Jaat, S. Tilak, "Harmonic elimination of a fifteen-level inverter with reduced number of switches using genetic algorithm," IET Power Electronics, 2023, doi: 10.1049/pel2.12622.
- [14] T. K. S. Freddy, J.-H. Lee, H.-C. Moon, K.-B. Lee, N. A. Rahim, "Modulation Technique for Single-Phase Transformerless Photovoltaic Inverters With Reactive Power Capability," IEEE Transaction on Industrial Electronics, Vol. 64, No. 9, 2017, doi: 10.1109/TIE.2017.2686366.
- [15] T. Debela, J. Singh, V. K. Sood, "An assessment of Hbridge less grid-tied multilevel inverter with minimum

- device count and lesser total standing voltage," IET Power Electronics, 2023, doi: 10.1049/pel2.12566.
- [16] Y. P. Siwakoti, F. Blaabjerg, "A Novel Flying Capacitor Transformerless Inverter for Single-Phase Grid Connected Solar Photovoltaic System," 2016 IEEE 7th International Symposium on Power Electronics for Distributed Generation Systems (PEDG), Canada, 2016, doi: 10.1109/PEDG.2016.7527086.
- [17] Y. P. Siwakoti, F. Blaabjerg, "H-Bridge Transformerless Inverter with Common Ground for Single-Phase Solar-Photovoltaic System," 2017 IEEE Applied Power Electronics Conference and Exposition (APEC), USA, 2017, doi: 10.1109/APEC.2017.7931066.
- [18] Y. P. Siwakoti, F. Blaabjerg, "Common-Ground-Type Transformerless Inverters for Single-Phase Solar Photovoltaic Systems," IEEE Transactions on Industrial Electronics, Vol. 65, No. 3, 2018, doi: 10.1109/TIE.2017.2740821.
- [19] M. N. H. Khan, M. Forouzesh, Y. P. Siwakoti, L. Li, T. Kerekes, F. Blaabjerg, "Transformerless Inverter Topologies for Single-Phase Photovoltaic Systems: A Comparative Review," IEEE Journal of Emerging and Selected Topics in Power Electronics, Vol. 8, No.1, 2020, doi: 10.1109/JESTPE.2019.2908672.
- [20] M. A. W. Begh, E. Liegmann, A. Mahajan, A. Palanisamy, Y. P. Siwakoti, P. Karamanakos, M. Abdelrahem, R. Kennel, "Design of State-Feedback Controller for a Single-Phase Grid-Connected Siwakoti-H Inverter with LCL filter," PCIM Europe 2019; International Exhibition and Conference for Power Electronics, Intelligent Motion, Renewable Energy and Energy Management, Germany, 2019.
- [21] M. A. W. Begh, E. Liegmann, P. Karamanakos, R. Kennel, "Direct Model Predictive Control of a Single-Phase Grid-Connected Siwakoti-H Inverter," IECON 2020 The 46th Annual Conference of the IEEE Industrial Electronics Society, Singapore, 2020, doi: 10.1109/IECON43393.2020.9255091.
- [22] M. A. W. Begh, E. Liegmann, P. Karamanakos, A. Mahajan, Y. P. Siwakoti, R. Kennel, "Indirect Model Predictive Control of a Three-Phase Grid-Connected Siwakoti-H Inverter," IECON 2019 - 45th Annual Conference of the IEEE Industrial Electronics Society, Portugal, 2019, doi: 10.1109/IECON.2019.8927830.
- [23] J. Slotine, W. Li, Applied Nonlinear Control, Pearson, 1991.

- [24] W. M. Haddad, V. S. Chellaboina, Nonlinear Dynamical Systems and Control: A Lyapunov-Based Approach, Princeton University Press, 2008, doi: 10.2307/j.ctvcm4hws.
- [25] C. M. Kellett, P. Braun, Introduction to Nonlinear Control: Stability, Control Design, and Estimation, Princeton University Press, 2023.



Amir Mohamad Mohamadi received his B.S. degrees in Electrical Engineering from Islamic Azad University of Najafabad, Isfahan, Iran, in 2002. He received his M.S. degree in electrical engineering from Iran University of Science and Technology, Tehran, Iran, in 2007. He is currently pursuing a Ph.D. in Electrical Engineering at Shahrekord University,

Shahrekord, Iran. His current research interests include power electronics and photovoltaic systems. His research aims to contribute to advancements in photovoltaic systems through energy efficiency and innovative control strategies.



Navid Reza Abjadi received the B.S., M.S., and Ph.D. degrees in electrical engineering from Isfahan University of Technology, Isfahan, Iran in 1999, 2001, and 2010 respectively. He is a lecturer at Shahrekord University. His research interests include motor drives, control theory applications, and

power electronics.



Gholamreza Arab Markadeh was born in Shahrekord, Iran, in 1974. He received the B.Sc., M.Sc., and Ph.D. degrees in Electrical Engineering from Isfahan University of Technology, Iran, in 1996, 1998, and 2005, respectively. He is currently a Professor in the Department of Electrical Engineering, Faculty of Engineering, Ferdowsi University of

Mashhad, Mashhad. His fields of research include nonlinear control, power electronics, and variable-speed drives. He is the Editor-in-chief of Journal of Dam and Hydroelectric Power plant. Dr. Arab Markadeh was the recipient of the IEEE Industrial Electronics Society IECON'04 best paper presentation award in 2004.